JBC RESEARCH ARTICLE

Identification of Rac guanine nucleotide exchange factors promoting Lgl1 phosphorylation in glioblastoma

Received for publication, December 7, 2020, and in revised form, August 25, 2021 Published, Papers in Press, October 6, 2021,
https://doi.org/10.1016/j.jbc.2021.101172

Sylvie J. Lavictoire[1], Danny Jomaa[1,2,3], Alexander Gont[4], Karen Jardine[1], David P. Cook[1,5], and Ian A. J. Lorimer[1,2,6,*]

From the [1]Cancer Therapeutics Program, Ottawa Hospital Research Institute, Ottawa, Ontario, Canada; [2]Department of Biochemistry, Microbiology and Immunology, University of Ottawa, Ottawa, Ontario, Canada; [3]School of Medicine, Faculty of Health Sciences, Queen's University, Kingston, Ontario; [4]Cell Biology Program, The Hospital for Sick Children, Toronto, Ontario, Canada; [5]Department of Cellular and Molecular Medicine and [6]Department of Medicine, University of Ottawa, Ottawa, Ontario, Canada

Edited by Alex Toker

The protein Lgl1 is a key regulator of cell polarity. We previously showed that Lgl1 is inactivated by hyperphosphorylation in glioblastoma as a consequence of *PTEN* tumour suppressor loss and aberrant activation of the PI 3-kinase pathway; this contributes to glioblastoma pathogenesis both by promoting invasion and repressing glioblastoma cell differentiation. Lgl1 is phosphorylated by atypical protein kinase C that has been activated by binding to a complex of the scaffolding protein Par6 and active, GTP-bound Rac. The specific Rac guanine nucleotide exchange factors that generate active Rac to promote Lgl1 hyperphosphorylation in glioblastoma are unknown. We used CRISPR/Cas9 to knockout PREX1, a PI 3-kinase pathway-responsive Rac guanine nucleotide exchange factor, in patient-derived glioblastoma cells. Knockout cells had reduced Lgl1 phosphorylation, which was reversed by re-expressing PREX1. They also had reduced motility and an altered phenotype suggestive of partial neuronal differentiation; consistent with this, RNA-seq analyses identified sets of PREX1-regulated genes associated with cell motility and neuronal differentiation. PREX1 knockout in glioblastoma cells from a second patient did not affect Lgl1 phosphorylation. This was due to overexpression of a short isoform of the Rac guanine nucleotide exchange factor TIAM1; knockdown of TIAM1 in these PREX1 knockout cells reduced Lgl1 phosphorylation. These data show that PREX1 links aberrant PI 3-kinase signaling to Lgl1 phosphorylation in glioblastoma, but that TIAM1 is also to fill this role in a subset of patients. This redundancy between PREX1 and TIAM1 is only partial, as motility was impaired in PREX1 knockout cells from both patients.

Glioblastoma is an incurable form of brain cancer. *De novo* glioblastoma is the most common type of glioblastoma, accounting for approximately 90% of cases. While *de novo* glioblastoma exhibits extensive heterogeneity both at the histological and molecular levels, comprehensive genetic analyses show that aberrant activation of the PI 3-kinase pathway occurs in almost all patients (1, 2). This occurs through partial or complete mutational inactivation of *PTEN*, amplification of the tyrosine kinase receptors *EGFR* or *PDGFRA* and/or activating mutations in PI 3-kinase. Mouse models show that central nervous system–specific *PTEN* haploinsufficiency, in a TP53-null background, generates a brain cancer that closely resembles human glioblastoma (3). Two key features that are present in the mouse and human disease are the highly invasive behavior of the cancer and the presence of a population of cancer cells with a neural stem cell–like phenotype. With respect to the latter, *PTEN* inactivation, together with *TP53* inactivation, represses differentiation of cultured neural stem cells (4), suggesting a direct role for PTEN in maintaining and/or expanding a population of neural stem cell–like cells in glioblastoma.

The *Drosophila* mutant lethal 2 giant larvae were identified almost 50 years ago (5). This mutant shows overgrowth of brain tissue leading to death at the larval stage. Detailed studies have shown that the brain phenotype is due to a failure of neuroblasts to differentiate: rather than undergoing asymmetric cell divisions to produce a neuroblast and a committed neural progenitor, neuroblasts undergo symmetric divisions to produce two neuroblasts (6). Transplantation studies showed that these neuroblasts were also invasive within the *Drosophila* central nervous system (5). The lethal giant larvae phenotype is caused by deletion of the gene encoding the protein Lgl, a double beta-propeller protein with cytoskeletal protein-like functions that include binding to membranes and to nonmuscle myosin II (7–10). Its activity is negatively regulated by phosphorylation, predominantly mediated by atypical protein kinase C (11). While initial studies suggested that phosphorylation caused a large conformational change in Lgl (12), recent crystallography studies have not supported this (7). Rather, these studies show that phosphorylation occurs on a surface loop that is rich in positively charged residues that mediate membrane association of Lgl. Phosphorylation directly counters membrane association by neutralizing this negatively charged region and also indirectly by preventing the lipid-binding-induced formation of an alpha-helical segment within this loop that arranges positively charged residues in a conformation that enhances their membrane interaction. Membrane association of Lgl is essential

* For correspondence: Ian A. J. Lorimer, ilorimer@ohri.ca.

to its role in asymmetric cell division. Accumulation of active, membrane-associated Lgl at the basolateral membrane of the *Drosophila* neuroblast induces the sequestration of committed neural progenitor fate determinants there (13). With a specific, coordinated mitotic spindle alignment, these fate determinants are then selectively incorporated into one daughter cell during cell division. Inactivation of Lgl by phosphorylation also prevents it from binding to nonmuscle-myosin II and repressing filament assembly, a function that is necessary for its repression of cell motility (10).

As mutational inactivation of Lgl in *Drosophila* causes a glioblastoma-like phenotype, we asked whether Lgl inactivation might also have a role in human glioblastoma. In humans, there are two genes encoding homologs of *Drosophila* Lgl, *LLGL1* and *LLGL2*. Neither of these is mutated in glioblastoma and *LLGL1*, encoding the protein Lgl1, and is expressed relatively abundantly. We explored the possibility that Lgl1 was instead inactivated by hyperphosphorylation. Consistent with this, we showed that *PTEN*-null glioblastoma cells had a high level of Lgl1 phosphorylating activity and that this was reduced upon restoration of PTEN expression (14). Introduction of a nonphosphorylatable, constitutively active version of Lgl1 repressed glioblastoma cell invasion and promoted its differentiation, both in cell culture and *in vivo* (15).

Lgl binds the scaffolding protein Par6; Par6 also binds aPKC, and it is this complex that mediates Lgl phosphorylation (16). Activation of aPKC is controlled by binding of a third protein to Par6, either activated (*i.e.*, GTP-bound) Cdc42 or Rac GTPases (17). Of the three Par6 protein family members (*PARD6A*, *PARD6B*, *and PARD6G*), TCGA RNA-Seq data suggests that *PARD6A* is the most highly expressed (1). Par6A, encoded by *PARD6A*, is able to bind both Cdc42 and Rac (17). Pull-downs of flag-tagged Par6A in glioblastoma cells showed that it predominantly associated with Rac1 (18). This association requires Rac1 activation by an Rac guanine nucleotide exchange factor (GEF). Here we have assessed the role of specific Rac GEFs in promoting the phosphorylation of Lgl1 in glioblastoma cells isolated from patients. We initially focused on the Rac GEF PREX1, which we previously showed was overexpressed in glioblastoma relative to normal brain (18). CRISPR/Cas9 knockout of PREX1 in glioblastoma cells from one patient showed markedly reduced Lgl1 phosphorylation, along with reduced motility and an apparent partial differentiation along the neuronal lineage. Knockout of PREX1 in cells from a second patient did not affect Lgl1 phosphorylation; these cells overexpressed a second Rac GEF, TIAM1, which was able to promote Lgl1 phosphorylation in the absence of PREX1, showing that there are redundant mechanisms for Lgl1 phosphorylation in a subset of glioblastoma patients. However, knockout of PREX1 in cells from both patients reduced motility, suggesting a nonredundant role for PREX1 in driving glioblastoma invasion.

Results

Generation of PriGO8A PREX1 knockout cells

PriGO8A cells are glioblastoma cells that were isolated from a patient undergoing surgery for glioblastoma. They were isolated and cultured in neural stem cell media using monolayer growth on laminin substrate and a 5% oxygen environment (14). Details of their neural stem cell–like properties and *in vivo* growth after intracerebral injection into immunocompromised mice have been described previously (14, 15). To knock out PREX1 in PriGO8A cells, complexes of Cas9, tracrRNA, and a crRNA targeting exon 2 of PREX1 were electroporated into cells as described in Experimental procedures. To produce a high frequency of mutated alleles, the electroporation was repeated 2 weeks later. Clonal populations were isolated using limiting dilution, with 29 wells in a 96-well plate giving cell populations. PriGO8A cells grow poorly at low densities: to compensate for this, clonal populations were isolated using conditioned media prepared as described in Experimental procedures. The mutation status of clones was assessed by TIDE analysis (19). The majority of isolated clones had a mixture of −5 and −2, consistent with clonal populations with biallelic PREX1 mutations. 8A/clone 4, along with a second clone with the same pattern of *PREX1* mutations (8A/clone 6), was chosen for further study (Fig. 1*A*). An additional population (8A/clone 18) had −5 and −2 deletions and +1 insertions (Fig. 1*A*). Although this is referred to as clone 18 here, this may be a mixed population of cells with different *PREX1* mutations. This was also chosen for initial further study as it lacked detectable wild-type *PREX1* alleles. Western blot analysis showed that the three clones did not express detectable PREX1 protein (Fig. 1*B*), and immunofluorescence analysis of 8A/clone 4 showed that PREX1 protein expression was uniformly absent from individual cells (Fig. 1*C*).

Lgl1phosphorylation in PREX1-null glioblastoma cells

The ability of PREX1-null clones to phosphorylate Lgl1 was compared with parental PriGO8A cells. As antibodies that detect endogenous Lgl1 phosphorylation are not available, PriGO8A cells were first transduced with flag-tagged Lgl to increase levels. Total cell lysates were then probed by Western blotting with an antibody that detects phosphorylated PKC substrates. As described previously, this detects a band of the expected size for Lgl1 (kDa) that is absent in untransduced cells and cells transduced with a version of Lgl1 in which the three hinge region serine residues are mutated to alanine (14); the band is also reduced by siRNA knockdown of Lgl1 and atypical PKCι (14). In the two PREX1-null clones examined here, levels of phosphorylated Lgl1 were consistently lower compared with PriGO8A parental cells (Fig. 2*A*). Levels of total transduced Lgl1 protein were also consistently lower, but quantitation showed that the overall extent of Lgl1 phosphorylation was still lower in the PREX1-null clones when this was corrected for (Fig. 2*B*).

Differences in Lgl1 phosphorylation could be explained by loss of PREX1 but could alternatively be due off-target effects of the crRNA, clonal variation, or changes due to the long-term passage of these cells that was necessary to isolate clonal populations. To determine if the changes were due to loss of PREX1, PREX1-null glioblastoma cells were genetically

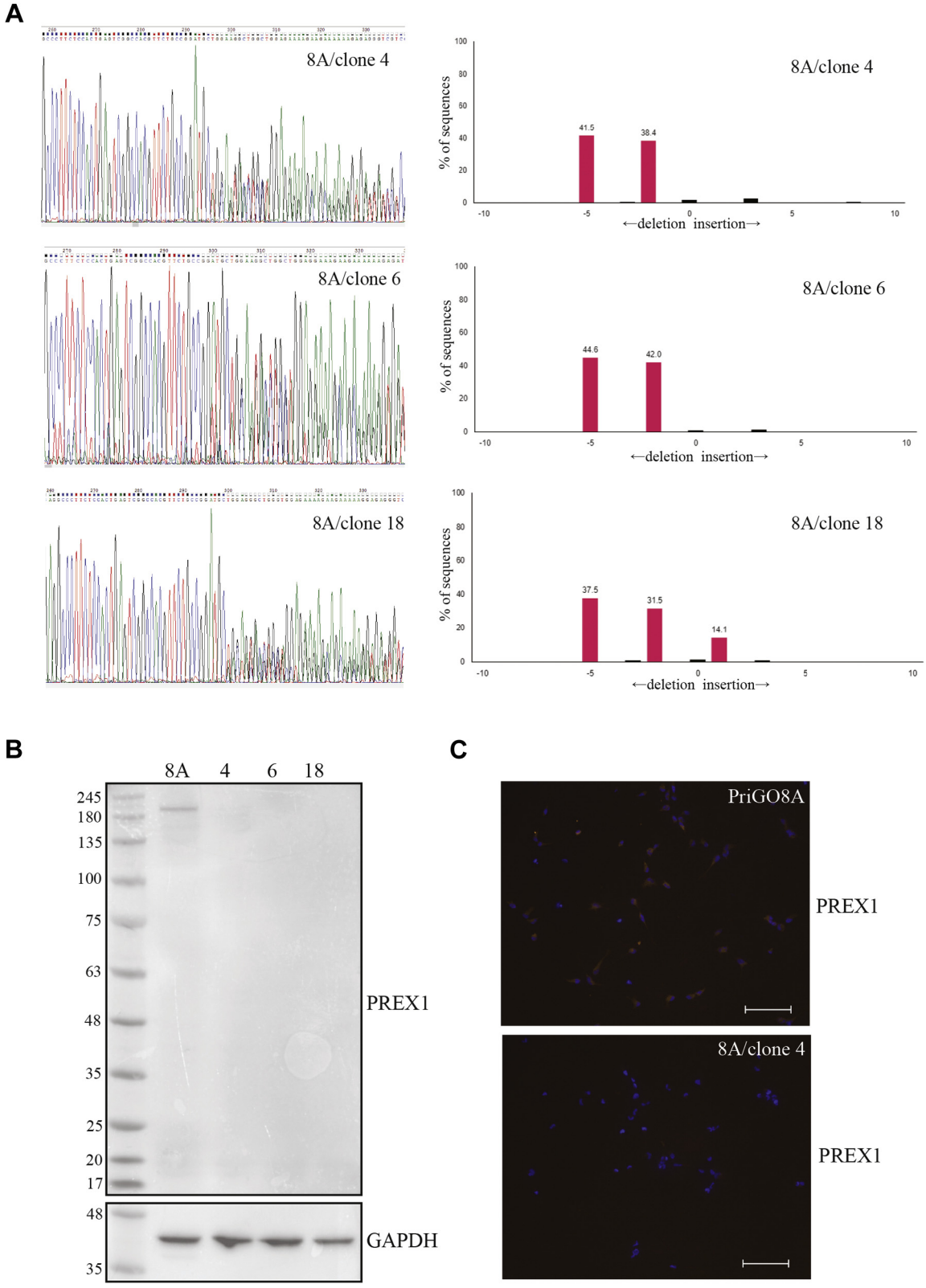

Figure 1. Generation of PREX1 knockout PriGO8A patient-derived glioblastoma cells. *A*, genomic analysis of PREX1 knockout cells. To determine deletions/insertions in clones isolated by limiting dilution, the targeted region of the *PREX1* gene was PCR amplified and sequenced (*left panels*). Sequence trace decomposition (*right panels*) was done using software described in Brinkman *et al.* (32). *B*, Western blot showing PREX1 expression in parental cells (8A) and three knockout clones. *C*, immunofluorescence for PREX1 on PriGO8A cells and clone 4. Scale bar is 100 μm.

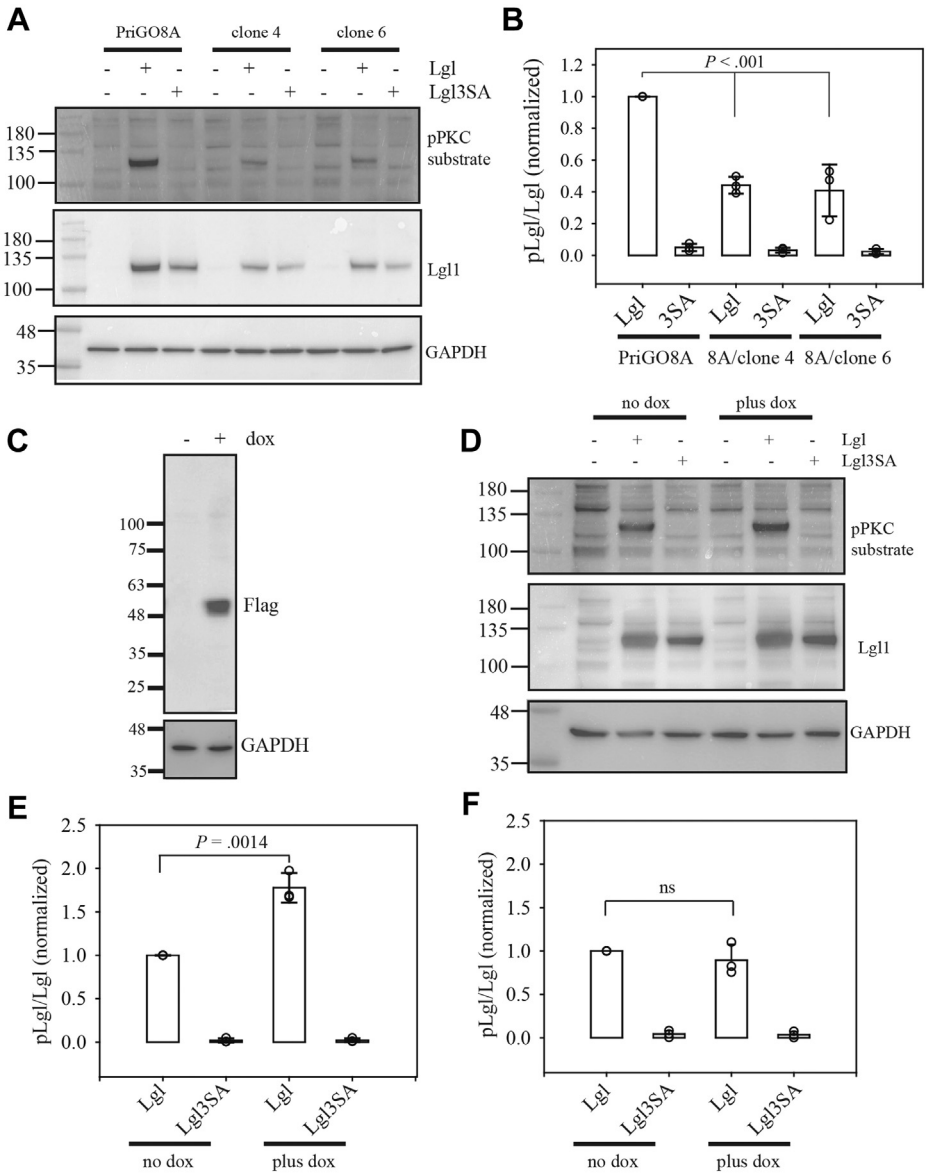

Figure 2. Lgl1 phosphorylation in PriGO8A and PREX1-knockout cells. *A*, PriGO8A cells and PREX1-null knockout clones 4 and 6 were untransduced, transduced with lentivirus expressing Lgl, or transduced with lentivirus expressing Lgl3SA. Two days later, samples were collected for Western blotting with antibody to phosphoPKC substrate, Lgl, and GAPDH. An example of a Western blot is shown. Antibodies used are shown on the *right-hand side* of each blot. Phosphorylated Lgl1 was detected with antibody to phosphoPKC substrate, total Lgl1 was detected with antibody to Lgl1, and antibody to GAPDH was used as a loading control. *B*, quantitative Western blot data from three biological replicates for the experiment described in (*A*). Individual *circles* show values from each experiment (in some cases these are overlapping). Overlaid bar graphs show mean and standard deviation. Data for each experiment were normalized to the pLgl/Lgl signal for PriGO8A cells transduced with Lgl. The *p* value was determined by One-Way Analysis of Variance/All Pairwise Multiple Comparison Procedures (Holm-Sidak method). *C*, induction of Flag-tagged PREX PHDH domain expression in PREX1-null cells. Transduced clone 4 cells were either untreated or treated for 48 with 1 μg/ml doxycycline. Cells were harvested and analyzed by Western blotting with anti-Flag antibody. *D*, PREX1-knockout cells transduced with lentiviral vectors for doxycycline-inducible expression of PREX1 were plated in the absence or presence of doxycycline. One day later, cells were untransduced, transduced with lentivirus expressing Lgl, or transduced with lentivirus expressing Lgl3SA. Two days later, samples were collected for Western blotting with antibody to phosphoPKC substrate, Lgl, and GAPDH. An example of a Western blot is shown. *E*, quantitative Western blot data for the experiment described in (*D*). Data for each experiment were normalized to the pLgl/Lgl signal for cells transduced with Lgl and not treated with doxycycline. The *p* value was determined with a two-tailed *t* test. *F*, same as in (*E*), except that the experiments were performed using PREX DHPH domain with an E56A mutation that inactivates its Rac guanine nucleotide exchange activity. ns, not significant.

modified for doxycycline-inducible expression of PREX1 (Fig. 2*C*). As the full-length 5 kb cDNA for PREX1 is beyond the capacity of the lentiviral system used here, lentivirus expressing only the DHPH domain of PREX1 (with a carboxy-terminal Flag tag) was made. This domain contains the Rac1 guanine nucleotide exchange factor activity and PIP3 binding functions of full-length PREX1 (20). It is activated by PIP3 binding, although it has higher basal activity than full-length PREX1 due to the loss of autoinhibitory domains carboxy terminal to the DH/PH domains (20, 21). Induction of PREX1 DHPH domain expression in the PREX1 knockout cells reversed the reduction in Lgl1 phosphorylation, consistent with this effect being due to PREX1 knockout (Fig. 2, *D* and *E*). A mutant version of the PREX1 DHPH domain, in which the

guanine nucleotide exchange activity is disrupted by a E56A mutation (22), did not promote Lgl1 phosphorylation (Fig. 2*F*). The ability of constitutively active Rac1 to phosphorylate Lgl1 was also assessed. Induced expression of constitutively active Rac1 did not detectably increase overall Rac1 levels in PREX1 knockout cells (likely due to high endogenous levels), but did increase levels of activated Rac1 (Fig. 3, *A* and *B*). Constitutively active Rac1 also reproducibly increased Lgl1 phosphorylation (Fig. 3*C*).

Morphology motility and differentiation state of PREX1null cells

Phase-contrast video microscopy of multiple PREX1-null clones showed that they had an altered morphology with numerous thin branched extensions that extended and retracted dynamically (Fig. 4*A* and Videos S1–S4). PREX1-null cells exhibited very few lamellipodia, which are frequently present in parental cells. Live cell imaging of actin dynamics using Lifeact (23) made these differences more apparent (Fig. 4*B* and Videos S5 and S6). In addition, this demonstrated that the abundant microspikes/filopodia that are present in parental PriGO8A cells are absent in PREX1 knockout cells (Fig. 4*B*). Induction of PREX1 reversed the morphological changes seen in PREX1-null cells, with cells showing fewer neurite-like extensions and abundant lamellipodia (Fig. 5*A* and Videos S7 and S8). PREX1-null glioblastoma cells have reduced motility, as expected based on our earlier study (18) (Fig. 5*A* and Videos S1–S4). Induction of PREX1 reversed this loss of motility (Fig. 5*B* and Videos S7 and S8).

As the morphology of PREX1-null clones was suggestive of partial differentiation along the neuronal lineage, the expression of doublecortin, a marker of committed neural progenitors/immature neurons (24), was assessed. Western blot analysis showed that PREX1 knockout cells expressed increased levels of doublecortin (Fig. 5*C*). Consistent with data from other glioblastoma cells isolated under serum-free conditions (25), PriGO8A cells undergo differentiation along the astrocytic, but not the neuronal, lineage when treated with BMP4 (26). To determine if PREX1-null glioblastoma cells had lost their multilineage potential, we treated them with BMP4. Although control PriGO8A cells became positive for GFAP expression as expected, PREX1 null cells did not. (Fig. 5*D*). The morphology changes, doublecortin expression and loss of ability to differentiate along the astrocytic lineage are all consistent with PREX1-null cells having undergone partial neuronal differentiation.

RNA-seq analysis of PREX1 knockout cells

To further characterize PREX1-null glioblastoma cells, RNA-seq analyses were performed, comparing parental

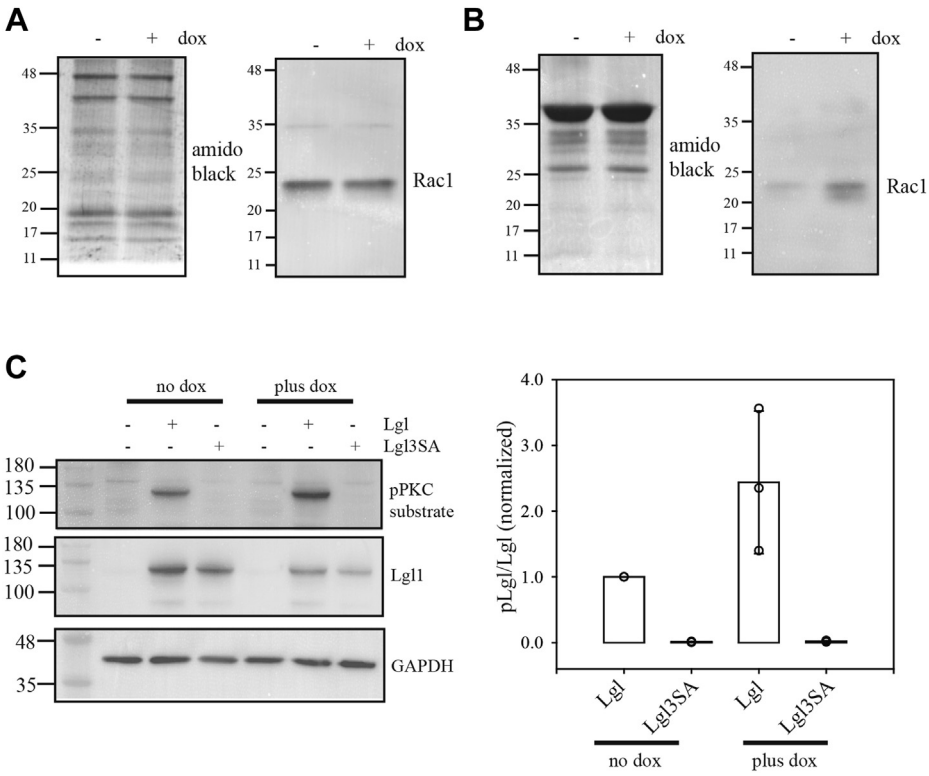

Figure 3. Lgl1 phosphorylation in PREX1-knockout cells expressing constitutively active Rac1. PREX1-null knockout clone 4 cells were transduced with lentiviral vectors for doxycycline-inducible expression of constitutively active Rac1. *A*, total cell lysates from cells treated without or with doxycycline for 48 h. The *left panel* shows amido black staining of the blot as a loading control. The *right panel* shows the same blot probed for Rac1. *B*, Rac1 activity assay for cells treated without or with doxycycline for 48 h. Active Rac1 pulldowns were done using GST-PAK1-PBD fusion protein. *Left panel* shows amido black staining as a loading control. *Right panel* shows the same blot probed for Rac1. *C*, effects of Lgl1 phosphorylation assays were performed as in Figure 2, *D* and *E*, except that cells with doxycycline-inducible expression of constitutively active Rac1 were used. An example Western blot is shown on the *left*. The plot on the *right* shows quantitative Western blot results from three biological replicates, with individual *circles* showing values from each experiment.

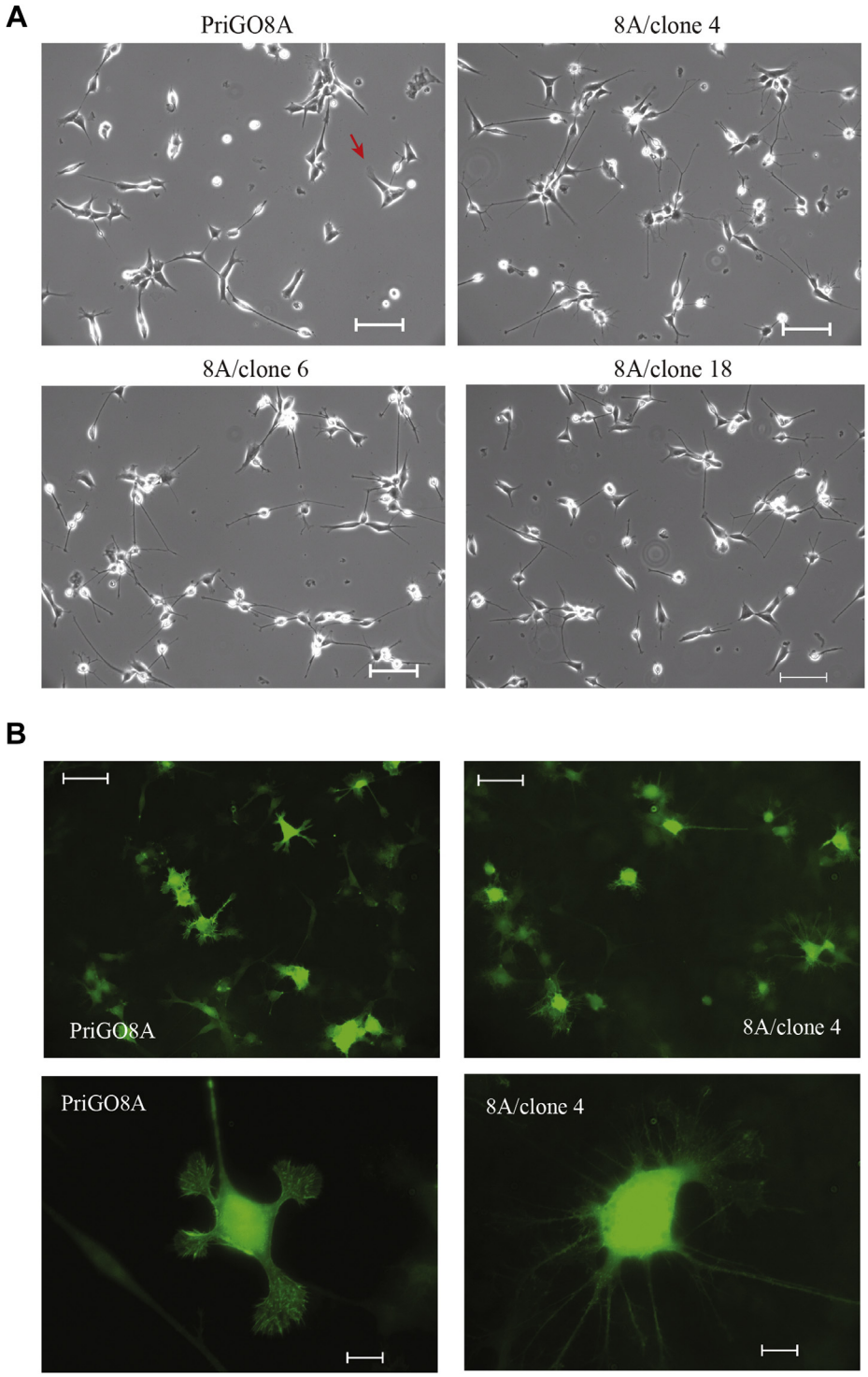

Figure 4. Morphology of PREX1-knockout PriGO8A cells. *A*, live cell phase-contrast images of PriGO8A and clones 4, 6, and 18. Scale bars are 200 μm. *Red arrows* indicate examples of lamellipodia. *B*, live cell imaging of actin dynamics in PriGO8A cells and clone 4 knockout cells. Scale bar for *top panels* is 100 μm. Scale bar for *bottom panels* is 20 μm. Full microscopy videos for A and B are shown in the Videos S1–S6.

PriGO8A cells with 8A/clone 4 cells and also comparing 8A/clone 4 cells with doxycycline-inducible PREX1, without and with 48 h doxycycline treatment. Each analysis was performed on two biological replicates. Figure 6*A* shows the number of genes with significantly changed expression in the two analyses at different cutoffs. In the PriGO8A:8A/clone 4 comparison, there were a large number of gene changes, with more genes downregulated than upregulated. In the comparison of 8A/clone 4/inducible PREX1 cells without and with doxycycline treatment, a much smaller number of genes showed changed expression, with upregulated genes predominating. These patterns are consistent with clone 4 cells having undergone

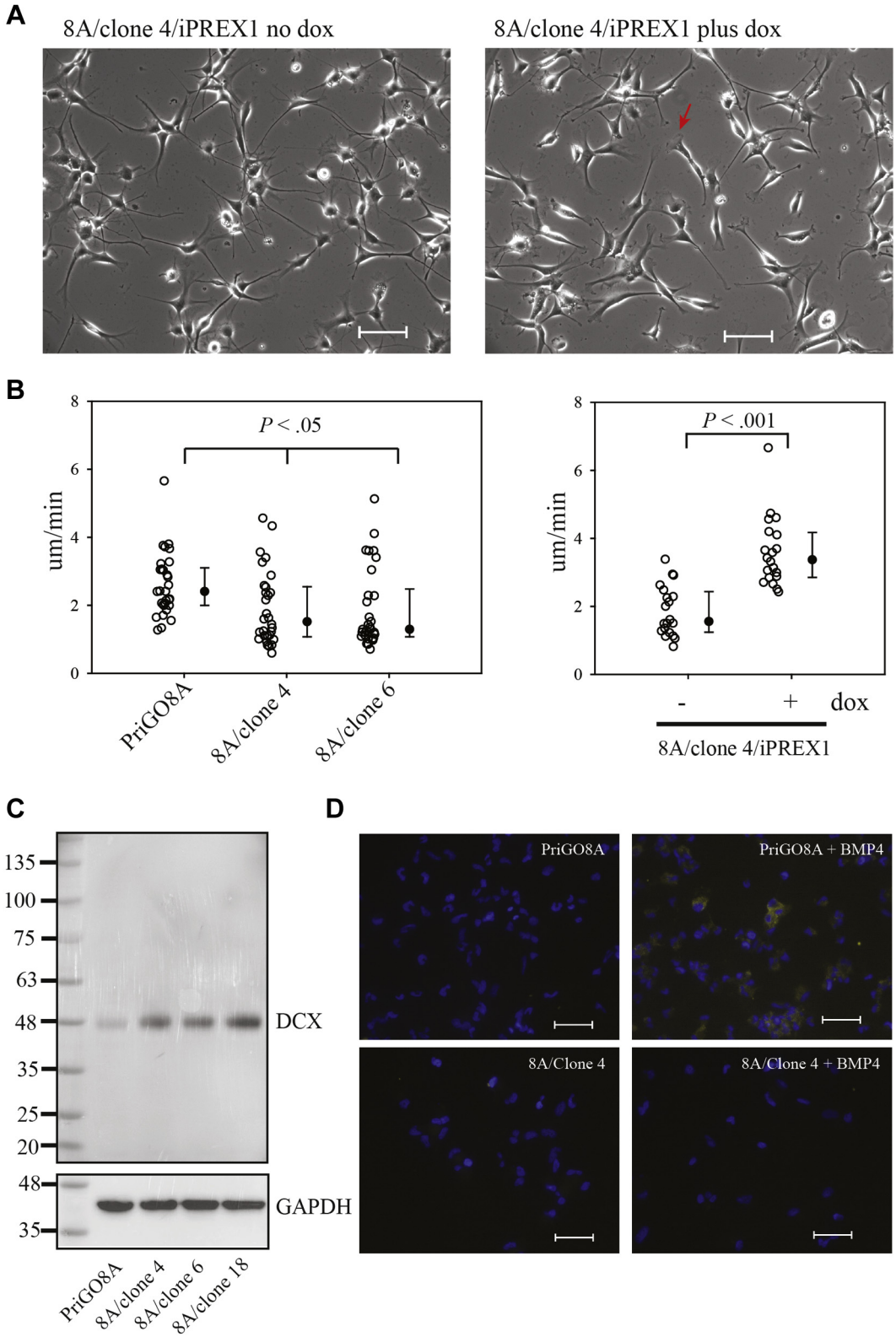

Figure 5. Changes in motility and differentiation state in PriGO8A PREX1-knockout cells. *A*, live cell phase-contrast images of PriGO8A PREX1-knockout cells transduced with lentiviral vectors for doxycycline-inducible PREX1 and grown in the absence or presence of doxycycline. Scale bars are 200 μm. The *red arrow* indicates an example of a lamellipodium. Full microscopy videos are shown in the Videos S7 and S8. *B*, motility of PREX1-null clones 4 and 6 (*left*) and PREX1-null clone 4 cells with re-expression of PREX1 (*right*). The *y* axis shows rate of movement in μm/min. *Open circles* show data for individual cells (30 per cell type in *right plot*; 20 per condition in *left plot*). Medians, 25th and 75th percentiles are shown to the *right* of individual cell data. The *p* value for the plot on the *left* was determined using the Kruskal–Wallis One-Way Analysis on Ranks/All Pairwise Multiple Comparison Procedures (Tukey Test). The *p* value for the plot on the *right* was determined using the Mann–Whitney Rank Sum test. See also Videos S1–S6. *C*, total cell lysates from PriGO8A cells and three knockout clones were analyzed for expression of doublecortin by Western blot analysis. *D*, PriGO8A and 8A/clone 4 cells were treated with 100 ng/ml BMP4 for 6 to 7 days. Cells were then fixed and immunofluorescence for GFAP was performed. Scale bar is 100 μm.

partial differentiation (large number of expression changes, with downregulation predominating due to cell specialization) and short-term activation of a specific signaling pathway in clone 4/DHPH treated with doxycycline. PREX1 mRNA levels were significantly lower in clone 4 (b = −0.55), potentially due to either changes in transcription or nonsense-mediated decay. Recent work has shown that gene knockouts can have compensatory increases in transcription of related genes by a mechanism that involves nonsense-mediated decay (27). However, changes in PREX2 mRNA, the gene most closely related to PREX1, were not observed, showing that this compensatory mechanism is not active in the PREX1 knockouts. With the inducible system, after 48 h treatment with doxycycline, PREX1 mRNA expression was 3-fold higher than in parental PriGO8A cells.

Figure 6*B* shows the intersection of the data sets from the RNA-seq analyses for PREX1 and knockout and restoration, using the qval <0.01 cutoff for both. This identified a set of 153 genes that are significantly altered (*i.e.*, both increased and decreased expression) in both analyses. This set should identify genes that are regulated relatively directly by PREX1, although it will exclude PREX1-regulated genes where expression is only transient due to feedback inhibition or other factors. The set will also exclude differences due to clonal selection of clone 4 from the parental PriGO8A population and possible nonspecific effects of doxycycline on gene expression. Analysis of the 153 gene set for GO biological processes using Enrichr gave three matches that were significant by Enrichr-assigned adjusted *p* values (excluding matches with less than five genes). These were "regulation of cell migration," "negative regulation of neurogenesis," and "positive regulation of cell motility" (Fig. 6, *C–E*).

Although the number of genes associated with negative regulation of neurogenesis was small, it notably included *ASCL1*, which has a well-known role in promoting neurogenesis (28).

PREX1 knockout in glioblastoma cells from a second patient (PriGO9A)

For comparison, PREX1-null cells were generated in glioblastoma cells from a second patient, PriGO9A cells. The basic properties of PriGO9A cells were described previously (14). Six clones generated by limiting dilution were screened. Five of the six showed weak expression of PREX1 by Western blot; TIDE analysis showed that the majority of these had biallelic mutations of PREX1, but also a significant signal for wild-type PREX1. One clone was identified that had no signal by Western blot and had triallelic mutations for *PREX1* (1, 2, and 4 base pair deletions, Fig. 7*A*). Based on this, PriGO9A cells likely have three copies of the *PREX1* gene. This occurs in 37% of glioblastomas as a result of gain of an entire copy of chromosome 20 (29). In contrast to the findings with PREX1 knockouts in PriGO8A cells, PREX1-null PriGO9A cells did not have reduced levels of phosphorylated Lgl1 (Fig. 7*B*) and did not show an obvious change in morphology (Fig. 8*A* and Videos S9 and S10). They did however show reduced motility that was restored upon re-expression of PREX1 (Fig. 8*B*); video microscopy showed that while they extend small lamellipodia, these retract without productive cell movement (Videos S11 and S12).

One explanation for the differences between PriGO8A and PriGO9A PREX1 knockouts is that PriGO9A expressed high levels of a second Rac GEF that can also promote Lgl1 phosphorylation. Analysis of microarray expression data from PriGO8A, PriGO9A, and two other patient-derived cultures (26) showed that PriGO9A cells expressed 5- to 12-fold higher levels of TIAM1 mRNA compared with cells from other patients (Fig. 9*A*). TIAM1 protein was also expressed at higher levels (Fig. 9*B*). Full-length TIAM1 is 1591 amino acids, with a predicted molecular weight of 178 kD. There is a small increase in a band of approximately this size, but most of the increase is in two smaller forms. As the antibody used recognizes a carboxy terminal region, these are likely amino terminal-truncated versions. Two of these, arising through alternate splicing, have been described (NP_001340613.1 and NP_001340614.1) with predicted molecular weights of 71 and 68 kD. These differ as to whether they include or exclude exon 20. PCR of PriGO8A and PriGO9A cDNA using primers that amplify from the start site to downstream of the exon 20 encoded sequence gave a single band of the expected size for inclusion of exon 20 (Fig. 9*C*); this identity was confirmed by Sanger sequencing of the PCR product. Thus PriGO9A cells primarily express the NP_001340613.1 transcript; the second band seen on Western blots is likely due to posttranslational modification. Analysis of TCGA data using TCGASpliceSeq (30) indicates that glioblastomas more frequently express codons 18 to 29 of TIAM1 compared with the upstream codons required for full-length TIAM1 expression. However, the average difference is less than 2-fold (comparing adjacent exons) (Fig. 9*D*), showing that the high ratio of splice variant expression relative to the mRNA expressing full-length PREX1 that is seen in PriGO9A cells is uncommon. Analysis across 152 patients from the TCGA database shows that PREX1 mRNA expression is much higher than TIAM1 mRNA expression in most patients (Fig. 8*E*), with high TIAM1 expression only being observed in a small subset of patients (Fig. 8*E*).

To determine if high TIAM1 expression was maintaining Lgl1 phosphorylation in the PriGO9A PREX1 knockout cells (9A/clone 18), RNA interference was used to deplete these cells of TIAM1. Initially a pool of siRNAs was used, which gave knockdown of the three major TIAM1 species. For further experiments, an siRNA from this pool that targets a 3′ region shared by common TIAM1 splice variants was used. This also gave knockdown of the three major TIAM1 species (Fig. 10*A*). TIAM1 knockdown significantly reduced Lgl1 phosphorylation in these cells (Fig. 10, *B* and *C*). As a control, the effects of knockdown in PriGO8A cells were also assayed. TIAM1 knockdown in these cells had no effect on Lgl1 phosphorylation (Fig. 10*D*). Overexpression of the TIAM1 short splice variant in PriGO8A/clone 4 PREX1 knockout cells gave a doublet similar to that seen in PriGO9A cells, although relative intensities of the bands differed and a weak third band was also

A

PriGO8A vs. 8A/clone 4

cutoff	qval<0.05	qval<0.01	qval<0.05 b>|1|	qval<0.01 b>|1|	qval<0.01 b>|2|
Total changed	5378	3781	1139	909	254
Total up	2184	1496	497	397	66
Total down	3194	2285	642	512	188

8A/clone 4/iPREX1 -/+ dox

cutoff	qval<0.05	qval<0.01	qval<0.05 b>|1|	qval<0.01 b>|1|	qval<0.01 b>|2|
Total changed	631	390	33	22	3
Total up	370	230	30	20	3
Total down	261	190	3	2	0

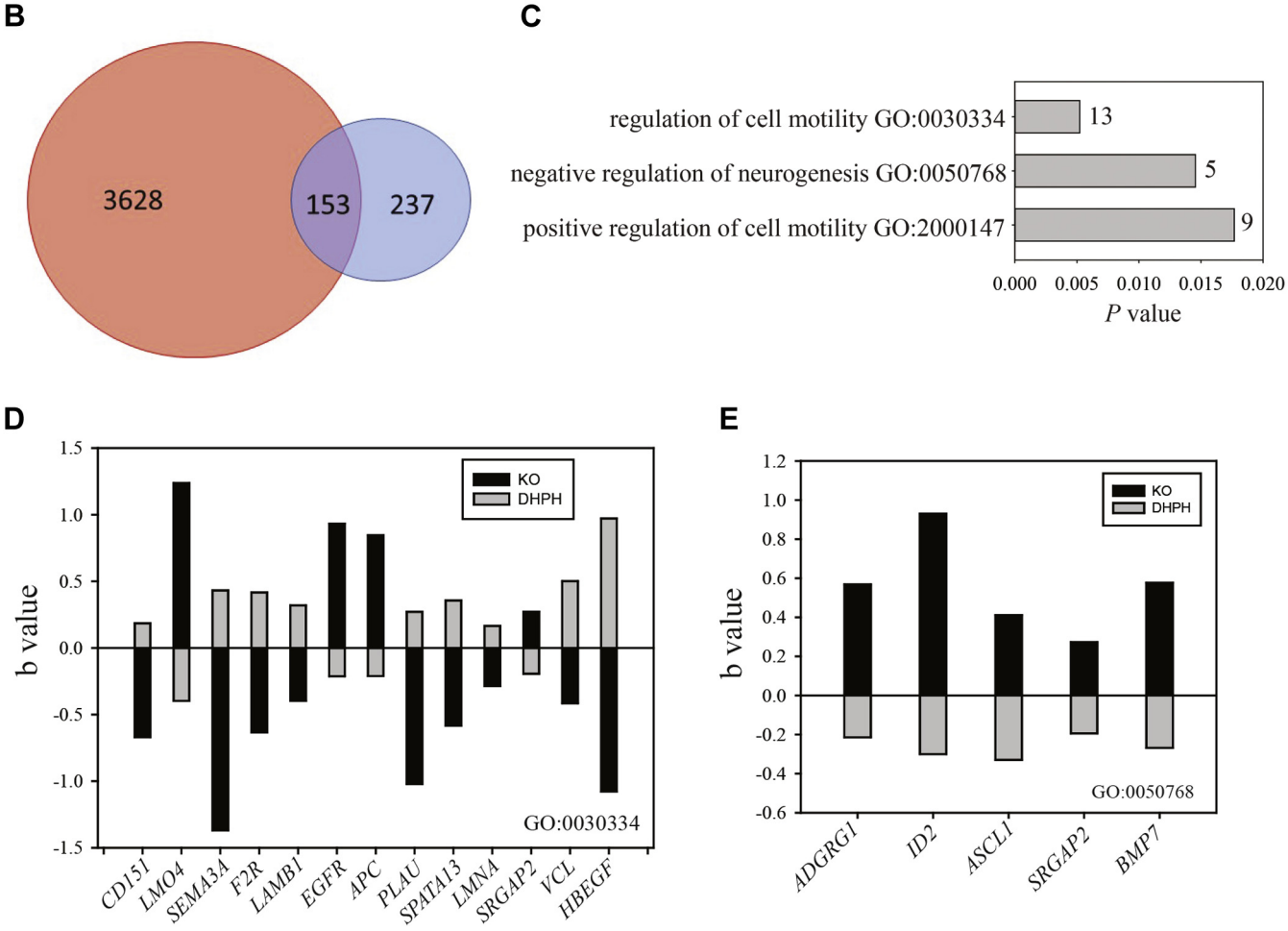

Figure 6. Changes in gene expression in PREX1 knockout cells. *A*, number of changes in gene expression using various cutoffs. q values (qval) are *p* values adjusted for multiple comparisons using the Benjamini–Hochberg FDR method. b values are estimates of effect size based on beta coefficients of the linear model fit to each gene and are expressed in log2. *B*, Venn diagram using qval <0.01 data for both RNA-seq experiments. *Red circle* shows the 3781 genes with altered expression at this cutoff in the comparison of PriGO8A cells with clone 4 PREX1 knockout cells. *Blue circle* shows the 390 genes with altered expression in clone 4 cells engineered for doxycycline-inducible PREX1, with and without 48 h doxycycline treatment. In total, 153 genes show altered expression in both data sets. *C*, analysis of gene ontology biological processes for 153 gene overlap using Enrichr[7]. GO terms are shown on the *y* axis and *p* values on the *x* axis. Numbers of genes associated with the GO terms are shown beside the bars. *D* and *E*, genes associated with GO terms for motility (*D*) and neurogenesis (*E*). *Black* bars show the change in expression between PriGO8A and 8A/clone 4 cells; *gray bars* show the change in expression in 8A/clone 4/iPREX1 cells without and with 48 induction of PREX1 expression with doxycycline.

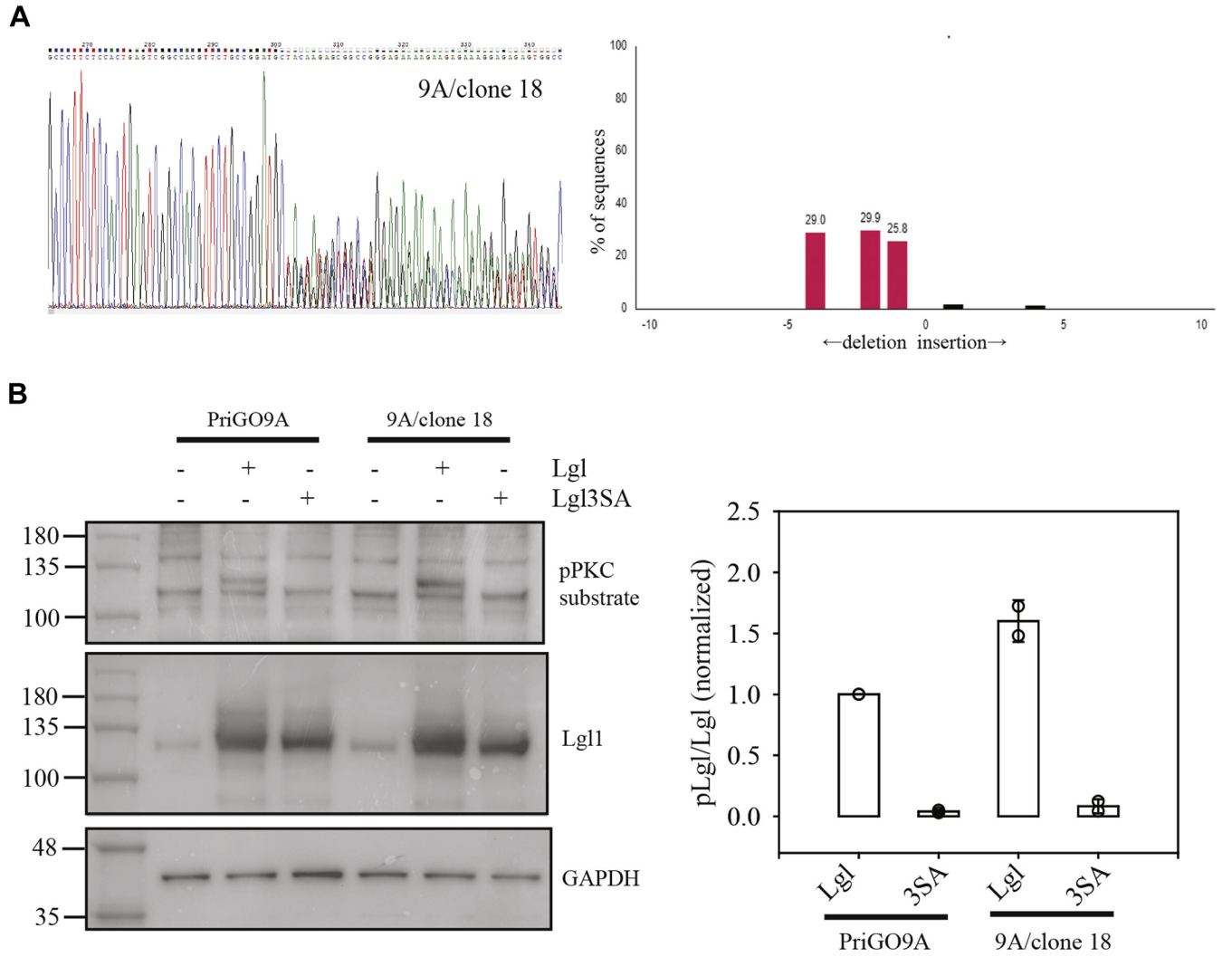

Figure 7. Generation of PREX1 knockout PriGO9A patient-derived glioblastoma cells. *A*, genomic analysis of PriGO9A PREX1 knockout cells was performed as described in Figure 1*A*. *B*, Lgl phosphorylation in PriGO9A and PriGO9A PREX1 knockout cells was performed as described in Figure 2*A*. The *open circles* show quantitative data from two separate experiments. Overlaid bar graphs show the mean and range. Data for each experiment were normalized to the pLgl/Lgl signal for PriGO9A cells transduced with Lgl.

observed (Fig. 10*E*). This also promoted Lgl1 phosphorylation, indicating that the TIAM1 short isoform is able to fulfill this role in other glioblastoma cells if its expression is artificially enhanced (Fig. 10*F*).

Discussion

Our previous work showed that inactivation of Lgl by phosphorylation has an important role in glioblastoma pathogenesis, where it is required both for the promotion of invasion and the repression of glioblastoma cell differentiation (15). Lgl phosphorylation was repressed when PTEN expression was restored in PTEN-null glioblastoma cells, showing a link between a common glioblastoma mutation and Lgl regulation (14). Here we have explored the role of Rac guanine nucleotide exchange factors in mediating signaling between the PI 3-kinase pathway and Lgl. We initially focused on PREX1, as it is directly regulated by PIP3 binding (31) and is overexpressed in glioblastoma (18). We used CRISPR/Cas9 to knockout PREX1 in PriGO8A glioblastoma cells. PriGO8A cells were isolated from a glioblastoma patient under conditions that preserve neural stem cell–like characteristics and are *PTEN*-null, C250T *TERT* promoter mutant, and without *EGFR* amplification (14). We were able to isolate clones that were confirmed to be PREX1-null by TIDE sequence analysis (19, 32) and Western blotting, showing that PREX1 is not essential for glioblastoma cell growth in cell culture. To determine Lgl phosphorylating activity in these cells, we transduced them with Lgl and then detected phosphorylation using an antibody to phosphoPKC substrate as described previously (14). Transduction in parallel with a non-phosphorylatable version of Lgl serves as a control in these assays. Lgl1 phosphorylation was significantly reduced in PREX1 knockout cells and could be restored by re-expressing PREX1, consistent with this effect being due to the knockout. This identifies a novel role for PREX1 as a regulator of polarity.

Live cell imaging showed that PREX1 knockout cells had reduced motility, in agreement with previous PREX1 siRNA

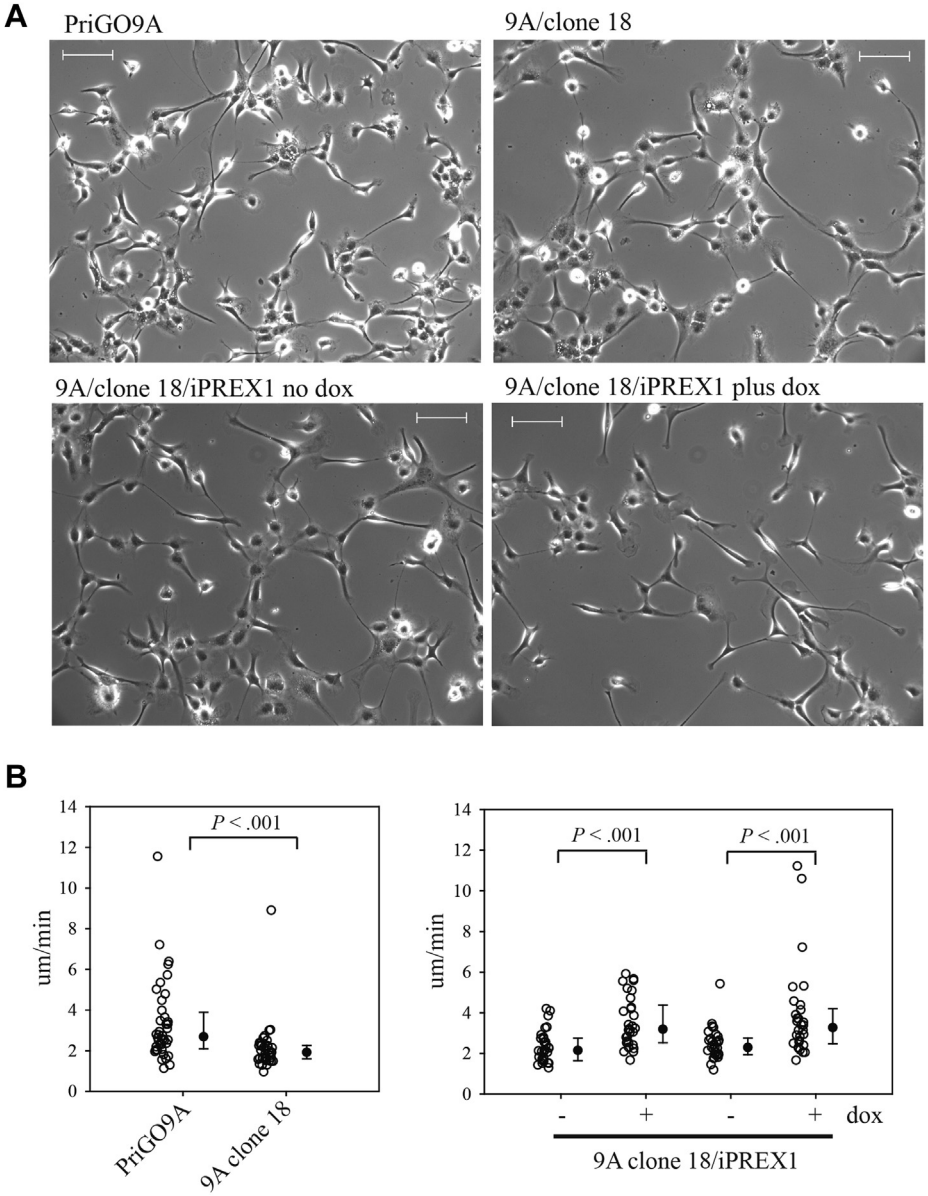

Figure 8. Morphology of PREX1-knockout PriGO9A cells. *A*, *top panels* show live cell phase-contrast images of PriGO9A (WT) and clone 18 (KO). *Bottom panels* show clone 18 cells transduced with lentiviral vectors for doxycycline-inducible expression of PREX1 and grown in the absence or presence of doxycycline. Scale bars are 200 μm. Full microscopy videos are shown in the Videos S7–S10 (*B*). The *left* bar graph shows the motility of PriGO9A and 9A clone 18 cells, while the *right panel* shows technical replicate experiments of 9A clone 18 cells with doxycycline-inducible PREX1. For both graphs, the *y* axis shows rate of movement in μm/min. *Open circles* show values for individual cells (40 per cell type on *left panel*; 30 per condition in *right panel*). Median, 25th and 75th percentiles are shown to the *right* of individual cell data. *p* values were determined using the Mann–Whitney Rank Sum test. See also Videos S7–S10.

knockdown experiments. Live cell imaging of actin dynamics confirmed the reduced lamellipodia formation and showed that microspike/filopodia formation was also impaired. The latter observation is consistent with a previous study of NIH3T3 cells overexpressing PREX1 (33). Both lamellipodia formation and motility were restored with induction of PREX1 expression, consistent with the alterations seen in knockout cells being due to PREX1 loss. Live cell imaging also showed that multiple PREX1 clones had an altered morphology, showing increased formation of thin, branched neurite-like extensions. This was suggestive of partial differentiation along the neuronal lineage. Consistent with this, knockout cells showed increased expression of the doublecortin, an early marker of neuronal differentiation; in addition, knockout cells no longer underwent astrocytic differentiation in response to BMP4 treatment, indicating a loss of multipotency. While some morphological changes are reversible, we have not fully evaluated the extent to which this partial differentiation is reversible, which will require a detailed epigenetic analysis. To further characterize PREX1 knockout cells, RNA-seq analysis of PriGO8A and 8a/clone 4 cells, as well as 8A/clone 4 cells with doxycycline-inducible PREX1, was performed. Analysis of the set of genes with changes in expression in both the PriGO8A: 8A/clone 4 comparison and the 8A/clone 4 without

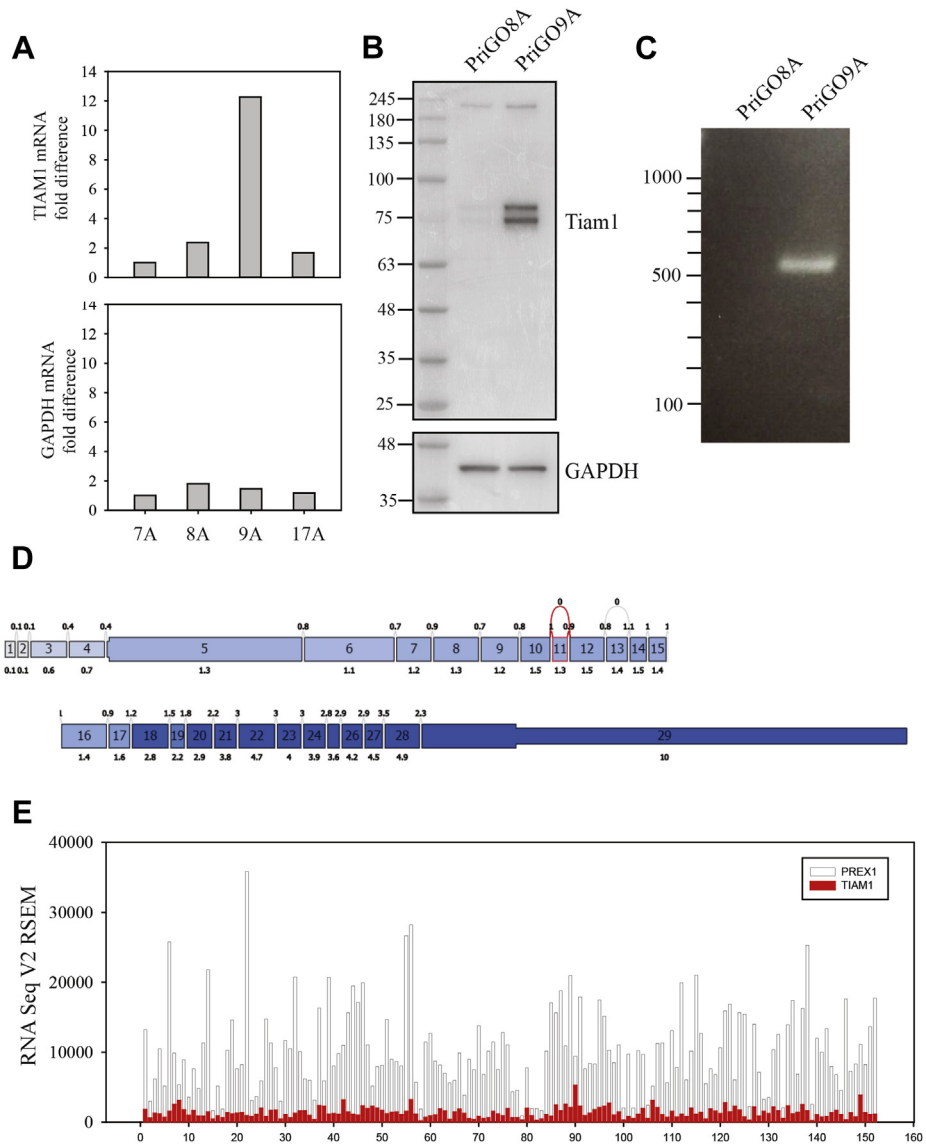

Figure 9. TIAM1 expression in glioblastoma. *A*, relative mRNA expression in glioblastoma cells from four patients (PriGO7A, PriGO8A, PriGO9A, and PriGO17A). Data are normalized to expression in PriGO7A. *B*, TIAM1 protein expression in PriGO8A and PriGO9A cells. Total cell lysates were analyzed by Western blotting. *C*, RT-PCR analysis of TIAM1 splice variant expression in PriGO9A cells. Equal amounts of PriGO9A and PriGO8A (as a control) mRNA were analyzed using a primer pair that spanned the exon 20 region that differs between the two reported splice variants encoding truncated isoforms of TIAM1. *D*, analysis of TIAM1 splice variants in glioblastoma from TCGA RNA-seq data. Data analysis and figure generation were done with TCGASpliceSeq (https://bioinformatics.mdanderson.org/public-software/tcgaspliceseq/). *Numbered boxes* show individual exons. *Upper numbers* show normalized read counts for splice events; *lower numbers* show normalized read counts for exon usage. The *shading* indicates expression level, with *darker blue* corresponding to higher expression. *E*, mRNA expression of PREX1 and TIAM1 from TCGA RNA-seq data. *y* axis shows normalized read counts. *x* axis shows individual patients (152 in total). *Clear* bars and *red* bars show PREX1 and TIAM1 expression, respectively.

and with PREX1 induction gave gene ontology signatures corresponding to regulation of cell motility and neurogenesis, consistent with the conclusions from the microscopy and marker expression analyses. For the motility signature, *HBEGF* is notable as its positive regulation by PREX1 potentially creates a positive feedback loop that could mediate a nonmotile/motile switch. Notable in the negative regulation of neurogenesis signature is *ASCL1*, which is known to undergo a switch from an oscillating to sustained expression during neural stem cell differentiation into committed progenitors (34).

To determine how generalizable the above findings were, we also generated PREX1 knockouts in glioblastoma cells from a second patient (PriGO9A cells). While PriGO8A cells appear to have two copies of PREX1, based on TIDE analysis, PriGO9A cells appear to have three copies, given that the one clone we isolated had three different deletions of roughly equal abundance. This is observed in 40% of glioblastomas and is due to chromosome 20 gain (29). In contrast to PriGO8A PREX1 knockout cells, PriGO9A knockout cells did not show reduced Lgl phosphorylation or morphological features suggestive of differentiation along the neuronal lineage. They did, however, show reduced motility that could be restored by re-expressing PREX1. We reasoned that the observed differences might be due to expression of another Rac GEF in these cells with partially overlapping functions. Inspection of

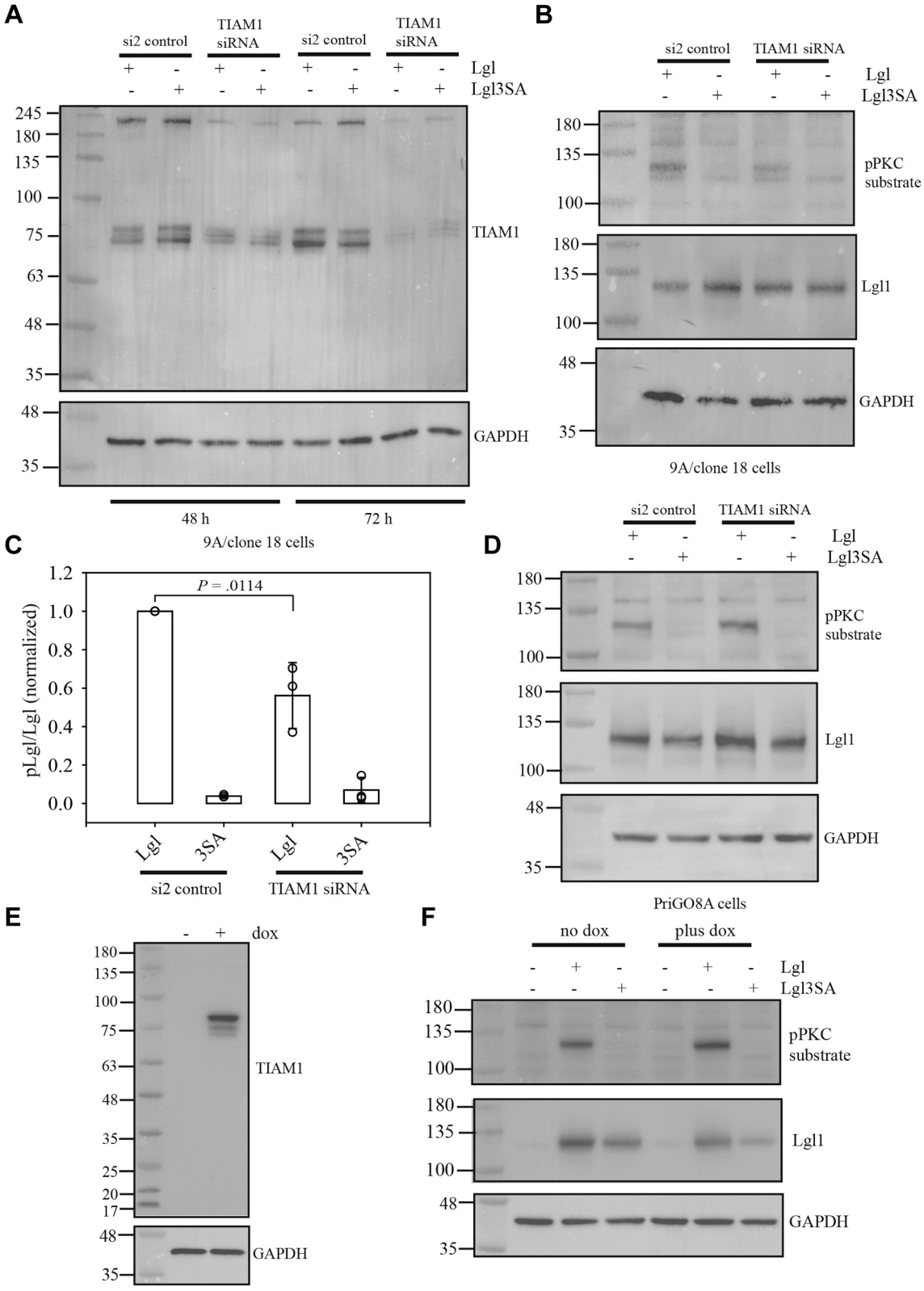

Figure 10. Effects of TIAM1 knockdown on Lgl phosphorylation. *A*, PriGO9A/clone 18 cells were transfected with a control siRNA (si2) or siRNA targeting TIAM1 1 day after plating. One or two days after plating, cells were transduced with lentiviral vectors expressing either Lgl or Lgl3SA. Three and four days after plating (48 or 72 h post siRNA transfection), total cell lysates were collected and analyzed by Western blotting for TIAM1. *B*, PriGO9A/clone 18 cells were treated as in (*A*). 72 h post siRNA transfection, total cell lysates were collected and analyzed by Western blotting for phosphoPKC substrate and Lgl. *C*, bar graph bar showing quantitative data from three biological replicates performed as in (*B*). Data were normalized as described in Figure 2*B*. *Open circles* show data from each replicate. Overlaid bar graphs show the mean and standard deviation. The *p* value was determined using the Mann–Whitney Rank Sum Test. *D*, the same experiment as shown in (*B*) was performed, except that PriGO8A cells were used. *E*, PriGO8A/clone 4 PREX1 knockout cells were transduced with lentiviral vector expressing the TIAM1 short splice variant. Cells were treated without or with doxycycline for 48 h to induce expression.

microarray data on these cells (26) showed that they expressed much higher mRNA levels of the Rac GEF TIAM1. TIAM1 has previously been linked to polarity regulation in keratinocyte tight junction biogenesis and neurite formation in neurons (35–38). Western blotting showed that TIAM1 protein was also expressed at high levels in these cells; however, this was an amino-terminal truncated form. PCR and sequencing showed that the overexpressed form was a previously identified splice variant of TIAM1 that encodes only the DH and PH2 domains of full-length TIAM1. Knockdown of TIAM1 in the PREX1 knockout PriGO9A cells, using an siRNA that targets mRNA for both full-length PREX1 and the shorter splice variant, reduced Lgl phosphorylation. Knockdown in PriGO8A cells, which express very low levels of TIAM1, had no effect on Lgl phosphorylation, consistent with the changes in PREX1 knockout PriGO9A cells being due to on-target effects of the siRNA. This second mechanism for Lgl1 phosphorylation is probably active in only a small subset of glioblastoma patients, based on analysis of exon expression levels and comparative RNA-seq expression of PREX1 and TIAM1 mRNA in 152 patients in the TCGA database. This splice variant of TIAM1 is expected to be constitutively active, as amino terminal truncation of TIAM1 is known to promote its stabilization and constitutive activation (39). In additional to *EGFR* amplification/mutation, *PTEN* loss, and other mutational mechanisms, this may provide an additional mechanism for partial growth factor independence in glioblastoma. Consistent with this, we previously reported that PriGO9A cells have a reduced propensity to differentiate after growth factor withdrawal compared with PriGO8A cells (14). This also suggests a role for alternate splicing in maintaining the malignant phenotype in a subset of glioblastomas.

As PREX1 requires PIP3 binding for its activation and the role of phosphorylation in regulating Lgl is well established, the experiments described here establish a new role for PREX1 in linking aberrant PI 3-kinase pathway signaling in glioblastoma to the disruption of normal polarity pathway signaling. While PREX1 knockout affected Lgl phosphorylation in one of the two patient-derived glioblastoma cells, motility was impaired in both, suggesting a nonredundant role for PREX1 in glioblastoma cell motility. Lgl phosphorylation, while necessary for motility (15), does not appear to be sufficient. Marei *et al.* (33) have shown that PREX1, but not TIAM1, binds the actin remodeling protein FLII and that this is necessary for Rac-dependent cell migration in NIH3T3 cells; this is a likely candidate for a second PREX1-dependent signaling event that is required for glioblastoma motility.

While PREX1 appears to have a role in motility that is nonredundant with other Rac GEFs, this is clearly not the case for its role in Lgl1 phosphorylation. As above, TIAM1 can redundantly fulfill this role in a subset of glioblastomas. Lgl1 phosphorylation could also be promoted artificially with constitutively active Rac1. Thus PREX1 promotes Lgl1 phosphorylation in glioblastoma by virtue of its high expression in glioblastoma compared with other Rac GEFs (29) along with its responsiveness to PI 3-kinase pathway signaling, rather than as a consequence of unique scaffolding functions.

Experimental procedures

Antibodies

The following antibodies were used: PREX1 (D808D) rabbit monoclonal, doublecortin rabbit polyclonal antibody, LLGL1 (D2B5A) rabbit monoclonal antibody; phospho-PKC Substrate Motif [(R/K)XpSX(R/K)] MultiMab rabbit monoclonal antibody mix; TIAM1 rabbit polyclonal antibody; doublecortin rabbit polyclonal antibody, all from Cell Signaling Technology; GAPDH mouse monoclonal from Abcam; Flag M2 mouse monoclonal antibody from Sigma-Aldrich.

Cell culture

Glioblastoma cells were isolated from patients undergoing first surgical tumor resection at The Ottawa Hospital as described previously (14). Cells were grown as monolayers on tissue culture plates coated with laminin (Sigma-Aldrich) using neurobasal A medium with B27 and N2 supplements and EGF and FGF2 (all from Thermo Fisher Scientific Inc). Cells were incubated in 5% O_2 and 5% CO_2 at 37 °C.

Generation of PREX1 knockout glioblastoma cells

Glioblastoma PREX1 knockout cells were generated by electroporation of preformed crRNA/tracrRNA/Cas9 complexes. For the crRNA:tracrRNA duplex, a crRNA sequence targeting exon 2 of *PREX1* (CGTTCTGCCGGATGCGATGC) was used (Dharmacon). This was combined with tracrRNA-ATTO 550 (IDT DNA Technologies) to a final duplex concentration of 44 μM to form the complete guide RNA complex. The complex was then heated at 95 °C for 5 min. To form the Cas9 solution, for each well, 0.3 μl of 61 μM Cas9 nuclease stock solution (IDT DNA Technologies) was combined with 0.2 μl of Resuspension Buffer R (IDT DNA Technologies). To form the crRNA:tracrRNA:Cas9 complex, for each well, 0.5 μl of crRNA:tracrRNA complex was combined with 0.5 μl of diluted Cas9 nuclease and incubated for 20 min at room temperature. PriGO8A cells, grown to 70 to 80% confluence, were then resuspended in Resuspension Buffer R to 500,000 cells per well. For each well, the following complex was prepared: 1 μl crRNA:tracrRNA:Cas9 complex, 9 μl cell suspension, and 2 μl of 10 μM electroporation enhancer (Alt-R Cas9 Electroporation Enhancer, IDT DNA Technologies). To prepare the Neon Transfection System for electroporation, the Neon Tube was filled with 3 ml of Electrolytic Buffer and inserted into the Neon Pipette Station. A Neon Tip was inserted into the Neon Pipette and 10 μl of the 12 μl solution available for each well was drawn into the tip. The Neon Pipette and Tip were inserted into the Pipette Station. The following electroporation parameters were used: 1050 V, 30 ms, and two pulses. After electroporation, cells were

Total cell lysates were then analyzed by Western blotting. *F*, An Lgl1 phosphorylation assay was performed as described in Figure 2*D*, except that PriGO8A/clone 4 PREX1 knockout cells expressing TIAM1 splice variant were used.

immediately plated on a laminin-coated 6-well plate. ATTO 550 fluorescence was verified 24 h later by fluorescence microscopy. Two weeks after the first round of electroporation, a second round was performed on the same cells with the same experimental setup and electroporation parameters.

Cloning by limiting dilution

Cells were diluted to a concentration of approximately one cell per 100 µl and plated in 96-well plates. Growth in 96-well plates was done using a 50:50 mixture of regular media and conditioned media from 48 h cultures of untreated PriGO8A cells.

TIDE assays

Genomic DNA was isolated using the Bio Basic All-4-One Genomic DNA MiniPrep Kit following the manufacturer's protocol including the RNase treatment (Bio Basic Inc). The region around the CRISPR PREX1 target site was PCR-amplified using the primer pair DPREX3F (5′-GCACAGAGGGAAAGTCTCGG-3′) and DPREX3R (5′-GCTGCTCCAGTGTGTTTAAGG-3′). Sanger sequencing of PCR products was performed and sequence data was analyzed using TIDE software (https://tide.nki.nl/) (32).

Western blotting

Western blotting was done as described previously (14). Blots were stained with amido black prior to probing with antibody, to confirm even transfer of proteins. Blots were probed with antibody to GAPDH as an additional loading control. Blots were imaged using a BioRad ChemiDoc Imaging System (BioRad).

Immunofluorescence

Immunofluorescence was done as described previously (40).

TERT promoter mutation analysis

The region of genomic DNA containing the TERT promoter region was PCR-amplified as described (41), and PCR products were Sanger sequenced as above.

Live cell video microscopy

Cells were plated on laminin-coated Bioptechs delta-T dishes. For the duration of video acquisition, cells were maintained in a sealed chamber at 37 °C and 5% CO_2. Phase-contrast images were taken at 10-min intervals for 90 min total. Images were acquired with the 10× objective of a Zeiss Axiovert 200M microscope equipped with an AxioCam HRm CCD camera (Zeiss). Motility was quantitated using the MtrackJ plugin (42) in ImageJ software (National Institutes of Health) as described previously (15). For live cell imaging and video microscopy of actin, lentiviral particles expressing eGFP-tagged Lifeact (23) were made and used to transduce glioblastoma cells. pLenti Lifeact-EGFP BlastR was a gift from Ghassan Mouneimne (Addgene plasmid # 84383).

Lgl1 phosphorylation assay

Lentiviral vectors expressing human flag-tagged Lgl1 and Lgl1(3SA) were described previously (14). Lentiviral particles were generated as described previously (14), concentrated using Lenti-X Concentrator (Takara) and resuspended in neurobasal A medium supplemented as above. Phosphorylation of Lgl1 was detected by Western blotting with phospho-PKC Substrate Motif antibody mix; the blot was then stripped and reprobed with Lgl1 antibody. Nontransduced cells and cells transduced with LLGL1(3SA) were used as negative controls in all assays.

RNA-seq

Total RNA was isolated using the GE Illustra RNA Spin Kit (Thermo Fisher Scientific) according to kit protocol including DNase treatment. RNA was eluted 2× with 40 µl of RNAse free water and stored at −80 °C. RNA concentration was assayed using a Nanodrop 1000 (Thermo Fisher Scientific) and diluted to be within range of RNA seq requirements. (∼100 ng/µl). RNA-seq libraries were generated from 250 ng of total RNA. The NEBNext Poly(A) Magnetic Isolation Module and cDNA synthesis was achieved with the NEBNext RNA First Strand Synthesis and NEBNext Ultra directional RNA Second Strand Synthesis Modules (New England BioLabs). Libraries were prepared using the NEBNext Ultra II DNA Library Prep Kit for Illumina (New England BioLabs). Paired-end 100 bp reads were performed on an Illumina HiSeq4000. Pseudo alignment and transcript quantification were performed with Kallisto (43), and differential expression was determined using Sleuth (44). Gene ontology analysis was performed using Enrichr (45, 46).

Lentiviral vector constructs

A plasmid with cDNA for full-length human PREX1 was obtained from Dr Heidi Welch (Babraham Institute). To make a lentiviral vector expressing the DH-PH domain of PREX1, the primers 5′-GGATCCATGGAGGCGCCCAGCGGCAGC-3′ and 5′-CATCTTTGTAATCGCCCATGACGTAGGCATCACGCTC-3′ were used to amplify the region coding for PREX1 DHPH domains. A second round of PCR was then done with the same 5′ primer and the 3′ primer 5′-GAATTCT CATTTGT CGTCATCATCTTTGTAATCGCCCATG-3′ to add codons for a carboxy terminal Flag tag and a stop codon. The final PCR product was subcloned into pMiniT 2.0 vector (New England BioLabs) and fully sequenced. cDNAs with the correct sequence were then subcloned into the doxycycline-inducible lentiviral vector pLVX-Tight-puro (Clontech) using BamH1 and EcoR1 restriction sites. Lentiviral particles were generated as described above. The PREX1 DHPH E56A mutant was made by PCR using the primer pair 5′ CTCTGCGTCCTCAACGCTATCTT GGGCACCGAG 3′ and 5′ CTCGGTGCCCAAGATAGCGTT GAGGACGCAGAG 3′. Lentiviral vector for expression of constitutively active Rac1 was made by subcloning the Rac1 Q61L sequence from pSLIK CA Rac1 (47), a gift from Sanjay Kumar (Addgene plasmid # 84605), into pLVX-Tight-puro. To make lentiviral vector expressing the TIAM1 splice variant,

PCR was used to amplify its sequence from PriGO9A-generated cDNA and to add compatible ends for subcloning into pLVX-Tight-puro using the NEBuilder HiFi DNA Assembly kit (New England BioLabs).

Rac1 activity assay

Active Rac1 levels were determined using the Active Rac1 Detection Kit from Cell Signaling Technology.

siRNA knockdown

SMARTpool siGENOME TIAM1siRNA and siGENOME human TIAM1 (7074) siRNA 5′ CAUUCAAUCCUGCGUGAUA 3′ from Dharmacon were used at final concentrations of 20 nM to knock down TIAM1 expression, as described previously (18).

Statistics

Statistical analyses were done using SigmaPlot 12.5 and SigmaPlot 14.5 software. Details of specific tests used are given in the figure legends.

Data availability

All data are within the manuscript or available upon request. RNA-Seq data has been deposited to the Gene Expression Omnibus database (GEO accession GSE162783).

Supporting information—This article contains supporting information.

Author contributions—A. G. and I. A. J. L. conceptualization; S. J. L. and I. A. J. L. data curation; I. A. J. L. formal analysis; I. A. J. L. funding acquisition; S. J. L., D. J., K. J., and D. P. C. investigation; S. J. L., D. J., A. G., K. J., and D. P. C. methodology; I. A. J. L. project administration; D. P. C. software; A. G. and I. A. J. L. supervision; I. A. J. L. writing–original draft; S. J. L., D. J., A. G., K. J., D. P. C., and I. A. J. L. writing–review and editing.

Funding and additional information—This work was supported by operating grant MOP-136793 from the Canadian Institutes of Health Research and an operating grant from the Cancer Research Society (to I. A. J. L.). D. J. was supported by a Queen Elizabeth II Graduate Scholarship in Science & Technology. D. P. C. is supported by a Canadian Institutes of Health Research Frederick Banting and Charles Best Canada Graduate Scholarships Doctoral Award.

Conflict of interest—The authors declare that they have no conflict of interest with this article.

Abbreviation—The abbreviations used are: GEF, guanine nucleotide exchange factor.

References

1. Brennan, C. W., Verhaak, R. G., McKenna, A., Campos, B., Noushmehr, H., Salama, S. R., Zheng, S., Chakravarty, D., Sanborn, J. Z., Berman, S. H., Beroukhim, R., Bernard, B., Wu, C. J., Genovese, G., Shmulevich, I., *et al.* (2013) The somatic genomic landscape of glioblastoma. *Cell* **155**, 462–477
2. Verhaak, R. G., Hoadley, K. A., Purdom, E., Wang, V., Qi, Y., Wilkerson, M. D., Miller, C. R., Ding, L., Golub, T., Mesirov, J. P., Alexe, G., Lawrence, M., O'Kelly, M., Tamayo, P., Weir, B. A., *et al.* (2010) Integrated genomic analysis identifies clinically relevant subtypes of glioblastoma characterized by abnormalities in PDGFRA, IDH1, EGFR, and NF1. *Cancer Cell* **17**, 98–110
3. Zheng, H., Ying, H., Yan, H., Kimmelman, A. C., Hiller, D. J., Chen, A. J., Perry, S. R., Tonon, G., Chu, G. C., Ding, Z., Stommel, J. M., Dunn, K. L., Wiedemeyer, R., You, M. J., Brennan, C., *et al.* (2008) p53 and Pten control neural and glioma stem/progenitor cell renewal and differentiation. *Nature* **455**, 1129–1133
4. Zheng, H., Ying, H., Yan, H., Kimmelman, A. C., Hiller, D. J., Chen, A. J., Perry, S. R., Tonon, G., Chu, G. C., Ding, Z., Stommel, J. M., Dunn, K. L., Wiedemeyer, R., You, M. J., Brennan, C., *et al.* (2008) Pten and p53 converge on c-Myc to control differentiation, self-renewal, and transformation of normal and neoplastic stem cells in glioblastoma. *Cold Spring Harb. Symp. Quant. Biol.* **73**, 427–437
5. Gateff, E., and Schneiderman, H. A. (1974) Developmental capacities of benign and malignant neoplasms of Drosophila. *Wilhelm Roux Arch. Entwickl. Mech. Org.* **176**, 23–65
6. Knoblich, J. A. (2010) Asymmetric cell division: Recent developments and their implications for tumour biology. *Nat. Rev. Mol. Cell Biol.* **11**, 849–860
7. Almagor, L., Ufimtsev, I. S., Ayer, A., Li, J., and Weis, W. I. (2019) Structural insights into the aPKC regulatory switch mechanism of the human cell polarity protein lethal giant larvae 2. *Proc. Natl. Acad. Sci. U. S. A.* **116**, 10804–10812
8. Dong, W., Zhang, X., Liu, W., Chen, Y. J., Huang, J., Austin, E., Celotto, A. M., Jiang, W. Z., Palladino, M. J., Jiang, Y., Hammond, G. R., and Hong, Y. (2015) A conserved polybasic domain mediates plasma membrane targeting of Lgl and its regulation by hypoxia. *J. Cell Biol.* **211**, 273–286
9. Strand, D., Unger, S., Corvi, R., Hartenstein, K., Schenkel, H., Kalmes, A., Merdes, G., Neumann, B., Krieg-Schneider, F., and Coy, J. F. (1995) A human homologue of the Drosophila tumour suppressor gene l(2)gl maps to 17p11.2-12 and codes for a cytoskeletal protein that associates with nonmuscle myosin II heavy chain. *Oncogene* **11**, 291–301
10. Dahan, I., Petrov, D., Cohen-Kfir, E., and Ravid, S. (2014) The tumor suppressor Lgl1 forms discrete complexes with NMII-A and Par6alpha-aPKCzeta that are affected by Lgl1 phosphorylation. *J. Cell Sci.* **127**, 295–304
11. Hong, Y. (2018) aPKC: The kinase that phosphorylates cell polarity. *F1000Res.* **7**. F1000 Faculty Rev-903
12. Betschinger, J., Eisenhaber, F., and Knoblich, J. A. (2005) Phosphorylation-induced autoinhibition regulates the cytoskeletal protein Lethal (2) giant larvae. *Curr. Biol.* **15**, 276–282
13. Homem, C. C., and Knoblich, J. A. (2012) Drosophila neuroblasts: A model for stem cell biology. *Development* **139**, 4297–4310
14. Gont, A., Hanson, J. E., Lavictoire, S. J., Parolin, D. A., Daneshmand, M., Restall, I. J., Soucie, M., Nicholas, G., Woulfe, J., Kassam, A., Da Silva, V. F., and Lorimer, I. A. (2013) PTEN loss represses glioblastoma tumor initiating cell differentiation *via* inactivation of Lgl1. *Oncotarget* **4**, 1266–1279
15. Gont, A., Hanson, J. E., Lavictoire, S. J., Daneshmand, M., Nicholas, G., Woulfe, J., Kassam, A., Da Silva, V. F., and Lorimer, I. A. (2014) Inhibition of glioblastoma malignancy by Lgl1. *Oncotarget* **5**, 11541–11551
16. Yamanaka, T., Horikoshi, Y., Sugiyama, Y., Ishiyama, C., Suzuki, A., Hirose, T., Iwamatsu, A., Shinohara, A., and Ohno, S. (2003) Mammalian Lgl forms a protein complex with PAR-6 and aPKC independently of PAR-3 to regulate epithelial cell polarity. *Curr. Biol.* **13**, 734–743
17. Joberty, G., Petersen, C., Gao, L., and Macara, I. G. (2000) The cell-polarity protein Par6 links Par3 and atypical protein kinase C to Cdc42. *Nat. Cell Biol.* **2**, 531–539
18. Gont, A., Daneshmand, M., Woulfe, J., Lavictoire, S. J., and Lorimer, I. A. (2017) PREX1 integrates G protein-coupled receptor and phosphoinositide 3-kinase signaling to promote glioblastoma invasion. *Oncotarget* **8**, 8559–8573

19. Brinkman, E. K., Kousholt, A. N., Harmsen, T., Leemans, C., Chen, T., Jonkers, J., and van Steensel, B. (2018) Easy quantification of template-directed CRISPR/Cas9 editing. *Nucleic Acids Res.* **46**, e58
20. Hill, K., Krugmann, S., Andrews, S. R., Coadwell, W. J., Finan, P., Welch, H. C., Hawkins, P. T., and Stephens, L. R. (2005) Regulation of P-Rex1 by phosphatidylinositol (3,4,5)-trisphosphate and Gbetagamma subunits. *J. Biol. Chem.* **280**, 4166–4173
21. Ravala, S. K., Hopkins, J. B., Plescia, C. B., Allgood, S. R., Kane, M. A., Cash, J. N., Stahelin, R. V., and Tesmer, J. J. G. (2020) The first DEP domain of the RhoGEF P-Rex1 autoinhibits activity and contributes to membrane binding. *J. Biol. Chem.* **295**, 12635–12647
22. Lucato, C. M., Halls, M. L., Ooms, L. M., Liu, H. J., Mitchell, C. A., Whisstock, J. C., and Ellisdon, A. M. (2015) The phosphatidylinositol (3,4,5)-trisphosphate-dependent Rac exchanger 1·Ras-related C3 botulinum toxin substrate 1 (P-Rex1·Rac1) complex reveals the basis of Rac1 activation in breast cancer cells. *J. Biol. Chem.* **290**, 20827–20840
23. Padilla-Rodriguez, M., Parker, S. S., Adams, D. G., Westerling, T., Puleo, J. I., Watson, A. W., Hill, S. M., Noon, M., Gaudin, R., Aaron, J., Tong, D., Roe, D. J., Knudsen, B., and Mouneimne, G. (2018) The actin cytoskeletal architecture of estrogen receptor positive breast cancer cells suppresses invasion. *Nat. Commun.* **9**, 2980
24. Ayanlaja, A. A., Xiong, Y., Gao, Y., Ji, G., Tang, C., Abdikani Abdullah, Z., and Gao, D. (2017) Distinct features of doublecortin as a marker of neuronal migration and its implications in cancer cell mobility. *Front. Mol. Neurosci.* **10**, 199
25. Piccirillo, S. G., Reynolds, B. A., Zanetti, N., Lamorte, G., Binda, E., Broggi, G., Brem, H., Olivi, A., Dimeco, F., and Vescovi, A. L. (2006) Bone morphogenetic proteins inhibit the tumorigenic potential of human brain tumour-initiating cells. *Nature* **444**, 761–765
26. Kumar, R., Gont, A., Perkins, T. J., Hanson, J. E. L., and Lorimer, I. A. J. (2017) Induction of senescence in primary glioblastoma cells by serum and TGFbeta. *Sci. Rep.* **7**, 2156
27. El-Brolosy, M. A., Kontarakis, Z., Rossi, A., Kuenne, C., Gunther, S., Fukuda, N., Kikhi, K., Boezio, G. L. M., Takacs, C. M., Lai, S. L., Fukuda, R., Gerri, C., Giraldez, A. J., and Stainier, D. Y. R. (2019) Genetic compensation triggered by mutant mRNA degradation. *Nature* **568**, 193–197
28. Chouchane, M., and Costa, M. R. (2019) Instructing neuronal identity during CNS development and astroglial-lineage reprogramming: Roles of NEUROG2 and ASCL1. *Brain Res.* **1705**, 66–74
29. Lorimer, I. A. (2019) Aberrant Rac pathway signalling in glioblastoma. *Small GTPases* **12**, 1–15
30. Ryan, M., Wong, W. C., Brown, R., Akbani, R., Su, X., Broom, B., Melott, J., and Weinstein, J. (2016) TCGASpliceSeq a compendium of alternative mRNA splicing in cancer. *Nucleic Acids Res.* **44**, D1018–D1022
31. Welch, H. C. (2015) Regulation and function of P-Rex family Rac-GEFs. *Small GTPases* **6**, 49–70
32. Brinkman, E. K., Chen, T., Amendola, M., and van Steensel, B. (2014) Easy quantitative assessment of genome editing by sequence trace decomposition. *Nucleic Acids Res.* **42**, e168
33. Marei, H., Carpy, A., Woroniuk, A., Vennin, C., White, G., Timpson, P., Macek, B., and Malliri, A. (2016) Differential Rac1 signalling by guanine nucleotide exchange factors implicates FLII in regulating Rac1-driven cell migration. *Nat. Commun.* **7**, 10664
34. Imayoshi, I., Isomura, A., Harima, Y., Kawaguchi, K., Kori, H., Miyachi, H., Fujiwara, T., Ishidate, F., and Kageyama, R. (2013) Oscillatory control of factors determining multipotency and fate in mouse neural progenitors. *Science* **342**, 1203–1208
35. Mertens, A. E., Rygiel, T. P., Olivo, C., van der Kammen, R., and Collard, J. G. (2005) The Rac activator Tiam1 controls tight junction biogenesis in keratinocytes through binding to and activation of the Par polarity complex. *J. Cell Biol.* **170**, 1029–1037
36. Leeuwen, F. N., Kain, H. E., Kammen, R. A., Michiels, F., Kranenburg, O. W., and Collard, J. G. (1997) The guanine nucleotide exchange factor Tiam1 affects neuronal morphology; opposing roles for the small GTPases Rac and Rho. *J. Cell Biol.* **139**, 797–807
37. Matsuo, N., Hoshino, M., Yoshizawa, M., and Nabeshima, Y. (2002) Characterization of STEF, a guanine nucleotide exchange factor for Rac1, required for neurite growth. *J. Biol. Chem.* **277**, 2860–2868
38. Mertens, A. E., Pegtel, D. M., and Collard, J. G. (2006) Tiam1 takes PARt in cell polarity. *Trends Cell Biol.* **16**, 308–316
39. van Leeuwen, F. N., van der Kammen, R. A., Habets, G. G., and Collard, J. G. (1995) Oncogenic activity of Tiam1 and Rac1 in NIH3T3 cells. *Oncogene* **11**, 2215–2221
40. Baldwin, R. M., Barrett, G. M., Parolin, D. A., Gillies, J. K., Paget, J. A., Lavictoire, S. J., Gray, D. A., and Lorimer, I. A. (2010) Coordination of glioblastoma cell motility by PKCiota. *Mol. Cancer* **9**, 233
41. Nonoguchi, N., Ohta, T., Oh, J. E., Kim, Y. H., Kleihues, P., and Ohgaki, H. (2013) TERT promoter mutations in primary and secondary glioblastomas. *Acta Neuropathol.* **126**, 931–937
42. Meijering, E., Dzyubachyk, O., and Smal, I. (2012) Methods for cell and particle tracking. *Methods Enzymol.* **504**, 183–200
43. Bray, N. L., Pimentel, H., Melsted, P., and Pachter, L. (2016) Near-optimal probabilistic RNA-seq quantification. *Nat. Biotechnol.* **34**, 525–527
44. Pimentel, H., Bray, N. L., Puente, S., Melsted, P., and Pachter, L. (2017) Differential analysis of RNA-seq incorporating quantification uncertainty. *Nat. Methods* **14**, 687–690
45. Chen, E. Y., Tan, C. M., Kou, Y., Duan, Q., Wang, Z., Meirelles, G. V., Clark, N. R., and Ma'ayan, A. (2013) Enrichr: Interactive and collaborative HTML5 gene list enrichment analysis tool. *BMC Bioinformatics* **14**, 128
46. Kuleshov, M. V., Jones, M. R., Rouillard, A. D., Fernandez, N. F., Duan, Q., Wang, Z., Koplev, S., Jenkins, S. L., Jagodnik, K. M., Lachmann, A., McDermott, M. G., Monteiro, C. D., Gundersen, G. W., and Ma'ayan, A. (2016) Enrichr: A comprehensive gene set enrichment analysis web server 2016 update. *Nucleic Acids Res.* **44**, W90–W97
47. MacKay, J. L., and Kumar, S. (2014) Simultaneous and independent tuning of RhoA and Rac1 activity with orthogonally inducible promoters. *Integr. Biol. (Camb)* **6**, 885–894